Carbon 146 (2019) 313–319

Contents lists available at ScienceDirect

Carbon

journal homepage: www.elsevier.com/locate/carbon

Bismuth mediated defect engineering of epitaxial graphene on SiC(0001)

Tingwei Hu [a, b], Dayan Ma [a], Qinglong Fang [a], Peng Zhang [c], Xiangtai Liu [a], Ran Wei [d], Yi Pan [a, ***], Kewei Xu [a, **], Fei Ma [a, b, *]

[a] State Key Laboratory for Mechanical Behavior of Materials, Xi'an Jiaotong University, Xi'an, 710049, Shaanxi, China
[b] Collaborative Innovation Center of Suzhou Nano Science and Technology, Xi'an Jiaotong University, Suzhou, 215123, Jiangsu, China
[c] The Military Representative Office in Xi'an Area, The Army Armament Department, Xi'an, Shaanxi, 710032, China
[d] School of Materials Science and Engineering, Zhengzhou University, Zhengzhou, 450001, China

ARTICLE INFO

Article history:
Received 6 December 2018
Received in revised form
27 January 2019
Accepted 4 February 2019
Available online 5 February 2019

Keywords:
Epitaxial graphene (EG)
Defect engineering
Scanning tunneling microscopy/spectroscopy

ABSTRACT

Structural defects are commonly undesirable in materials, however, atomic-level defect engineering is promising to improve the electronic, mechanical and chemical properties of graphene, if the density and types of defects could be well controlled. Herein, bismuth-mediated defect engineering method for epitaxial graphene (EG) grown on SiC(0001) is demonstrated. It is found that single defects and defect clusters could be facilitated by evaporating Bi atoms on SiC(0001) substrate before the standard EG preparation and, Bi atoms could be thoroughly cleaned away from the EG and the unwanted doping effects of Bi will be avoided by post-annealing at higher temperature. Scanning tunneling microscopy/spectroscopy characterization reveals the atomic structures, the electronic states and the Fermi level shift of flower-like, tube-like and point defects. This study sheds light on the metal-mediated formation of defects in graphene, and provides a practical defect engineering method.

1. Introduction

Defects in graphene are commonly undesirable since they might deteriorate the device performances, for instance, lowering the carrier mobility due to the additional scattering effect [1,2]. However, some particular defects or defect clusters of well-controlled concentration could be significantly beneficial, which have been utilized to tune the chemical [3–6], mechanical [7–10] or electronic properties of epitaxial graphene (EG) [11,12]. For example, vacancies could, not only as the scattering centers of charge carriers, limit the transport properties [13,14], but also as the reaction centers, improve the adsorption [15], nucleation [16,17] and assembly of molecules on surface [18]. The vacancies could also provide diffusion channels and thus facilitate the intercalation of metal atoms underneath graphene [19–21]. Bubbled structures of graphene on metals [22] could also affect the mechanical and electronic properties [16,18], and the electron-phonon coupling on graphene is enhanced or modified by the rippled nano-ribbons [23], and pseudo-magnetic field might be induced by the lattice strain in graphene nano-bubbles [24]. Therefore, engineering of defects is an effective strategy to tailor the physical properties of graphene, and therefore endows a great number of new applications [25–28].

Defects are usually produced as by-products during functionalization of graphene through chemical doping in CVD growth, or deliberately by energetic ion bombardment [29,30]. But dopant complexes or defect clusters are usually produced, which is unsuitable for atomic level engineering [31–33]. Some intrinsic atomic defects are involved in the epitaxial graphene on 6H-SiC(0001) through thermal decomposition of SiC at high temperature, which cannot be well controlled [34]. So a method to controlably generate defects is highly desirable. Bi dopants might be induced in EG layer if the SiC substrate which is used to fabricate EG is covered with Bi atoms [35], and the density and types of defects are dependent on the process parameters. Therefore, the atomic-level defects in EG/SiC(0001) might be produced and tuned by introducing Bi atoms into this system during the growth of EG. In

* Corresponding author. State Key Laboratory for Mechanical Behavior of Materials, Xi'an Jiaotong University, Xi'an, 710049, Shaanxi, China.
** Corresponding author.
*** Corresponding author.
E-mail addresses: yi.pan@mail.xjtu.edu.cn (Y. Pan), kwxu@mail.xjtu.edu.cn (K. Xu), mafei@mail.xjtu.edu.cn (F. Ma).

https://doi.org/10.1016/j.carbon.2019.02.014
0008-6223/

this work, the strategy is demonstrated, both in-plane point defects and off-plane nano-protrusions are evidenced and, the atomic structure and electronic states of the defects are characterized by scanning tunneling microscopy/spectroscopy (STM/STS). Owing to the wafer-size fabrication of high-quality EG Refs. [36,37] and the potential applications in electronics [38,39], the defect engineering method are of great significance for the future applications in electronics [40].

2. Experiments

The fabrication and characterization of EG were mainly conducted in a commercial ultra-high vacuum (UHV) system (Unisoku USM-1400) equipped with molecular beam epitaxy (MBE) and STM. n-type 6H-SiC(0001) wafer was purchased from Tanke Blue Semiconductor Co. Ltd. Annealing temperature was controlled by direct current power supply, and monitored by an optical pyrometer. The SiC substrate was degassed at 823 K for at least 8 h in UHV to thoroughly remove the surface adsorbents. For the normal fabrication, SiC substrate was annealed at 1623 K under UHV condition (5×10^{-10} Torr) for 10 min. For Bi-assisted fabrication, a few layers of Bi were deposited on SiC after degassing. The pretreatment under Bi-atom-flux is similar to the fabrication of Si-terminated $\sqrt{3} \times \sqrt{3}$ structure under Si-flux annealing [41]. Afterwards, the Bi-covered SiC substrate was annealed at high temperatures (1623–1723 K) under UHV condition for 5 min and cooled down within 1 min. Such annealing cycle was repeated 2–3 times until deposited Bi atom are removed by sublimation. High density of in-plane defects and a few off-plane defects are generated in graphene if annealed at 1623 K, but the off-plane defects will substantially increased if the annealing is conducted at higher temperature. Surface chemical composition was calibrated by XPS and shown in the Supporting Information, but the Bi signal is below the sensitivity of the equipment. STM images and STS spectra were acquired with electrochemically etched W tips at 77.2 K. The topographic images were taken at constant current (100 pA) mode. STS was performed at a constant height mode, typically the height was optimized at a tip bias of 0.5 V and a set-point current of 200 pA. An AC modulation to the tunneling current with a frequency of 1.03 kHz and an amplitude of 20 mV was added by an internal lock-in electronics. Each dI/dV-V curve is an average of more than 10 individual spectra. Image processing and data analysis were performed in the latest version of WsXM [42].

3. Results and discussion

Fig. 1(a)-1(b) show the morphology of EG fabricated through normal thermal annealing of SiC under UHV environment. The specimen is seemingly clean, only a few defects are observed on EG terrace under both positive (4.0 V) and negative bias (−4.0 V). Fig. 1(c) displays the atomically resolved structure of the intact graphene sheet. Fig. 1(d) shows the morphology of EG after annealing the Bi-covered SiC substrate at 1623 K. As compared to EG fabricated without Bi, many defects are induced due to the

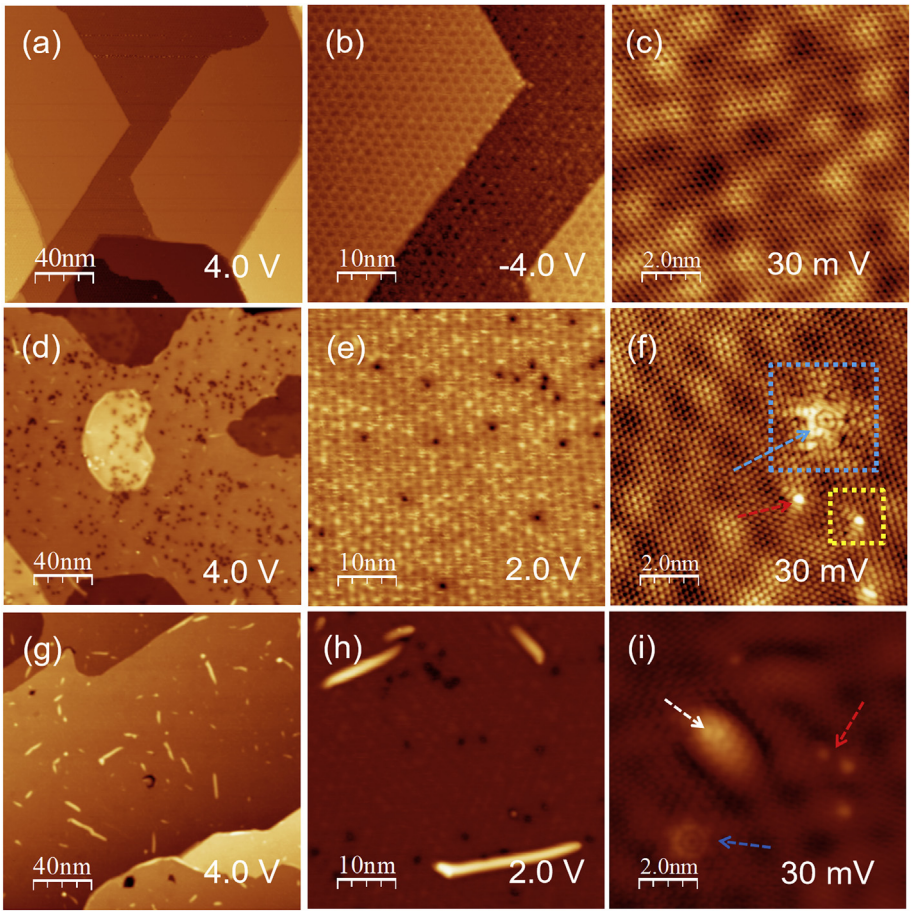

Fig. 1. (a)–(c) Morphology of EG produced by normal annealing process. (d)–(f) Morphology and defect structures of EG produced by annealing of Bi-covered SiC at 1623 K. (g)–(i) Morphology and defect structures of EG produced by annealing of Bi-covered SiC substrate at 1723 K. The tunneling current (I) of 100 pA is adopted, but with different bias voltage (V). (A colour version of this figure can be viewed online.)

participation of Bi atoms during the decomposition of SiC and the growth of EG, which are imaged as depressions and protrusions. Fig. 1(e) displays the detailed configurations of defects on EG, whereas, Fig. 1(f) shows the atomically resolved structures of two in-plane defects. The depressions under large positive bias voltages (4.0 V and 2.0 V) exhibit as in-plane tiny holes on EG, however, they can be distinguished as flower-like defects (blue arrow) and point defects (red arrow) under small bias (30 mV). Fig. 1(g)-1(i) show the morphology and atomic structure of defects on EG produced through annealing of Bi-pretreated SiC substrate at higher temperature of 1723 K. Except the in-plan defects, some off-plane protrusions are also observed. As shown by the atomic structure in Fig. 1(i), the off-plane protrusions are indeed ridged structures even under different bias voltages, and can be considered as tube-like defects (white arrow). More STM images obtained from different scanning regions are shown in Fig. S1 in the supplementary data.

Fig. 2(a) and (b) and 2(c) show the Raman spectra of the samples shown in Fig. 1(a) and (d) and 1(g), respectively, providing some macroscopic information about the quality of graphene. As shown in Fig. 2(a), the SiC peaks, G and 2D band of graphene are evidenced in EG sample produced by normal annealing process, but not the D-band, demonstrating high-quality EG produced. However, the D-band along with the G and 2D band is clearly observed in EG sample produced by annealing with the participation of Bi atoms [Fig. 2(b) and (c)]. Although it is hard to tell the defect type from Raman spectra, the appearance and the enhanced D-band is related to defects, indicating the increased defects to some degree. The density of all the defects on EG is evaluated to be about $0.5 \times 10^{12}/cm^2$. The density of point defects, flower-like defects, tube-like defects are significantly increased up to $4.8 \times 10^{12}/cm^2$, $1.0 \times 10^{12}/cm^2$, $0.6 \times 10^{12}/cm^2$, respectively, in EG produced on Bi-covered SiC substrate through annealing at 1623 K. The density of point defects and flower-like defects does not change substantially even at higher annealing temperature of 1723 K, while the density of tube-like defects is increased up to $3.8 \times 10^{12}/cm^2$. As displayed in Fig. S2, no Bi signal is detected in both the XPS spectra, although the pre-covered Bi atoms could not be thoroughly removed. That is, the concentration of Bi is below the detecting limit. Taking into account the high RSF value of Bi 4f (9.14), the concentration of Bi should be much lower than 0.1% on the surface. Additionally, a large number of atomic-resolution STM images taken randomly on the sample surface show that there are no Bi dopants in the graphene, which is consistent with the XPS spectra. Therefore, it can be concluded that the majority of Bi is sublimated, and the left Bi atoms might be dissolved into the bulk SiC and diluted.

Fig. 3(a) and (b) show the detailed structures of the two types of in-plane defects, which are zoomed in from the regions marked by blue and yellow squares in Fig. 1(f), respectively. The atomically resolved structure of the flower-like defect on EG layer is clearly evident in Fig. 3(a), which can be ascribed to the rotating sequence of dislocations (grain boundary loops) [43]. Because of the distorted

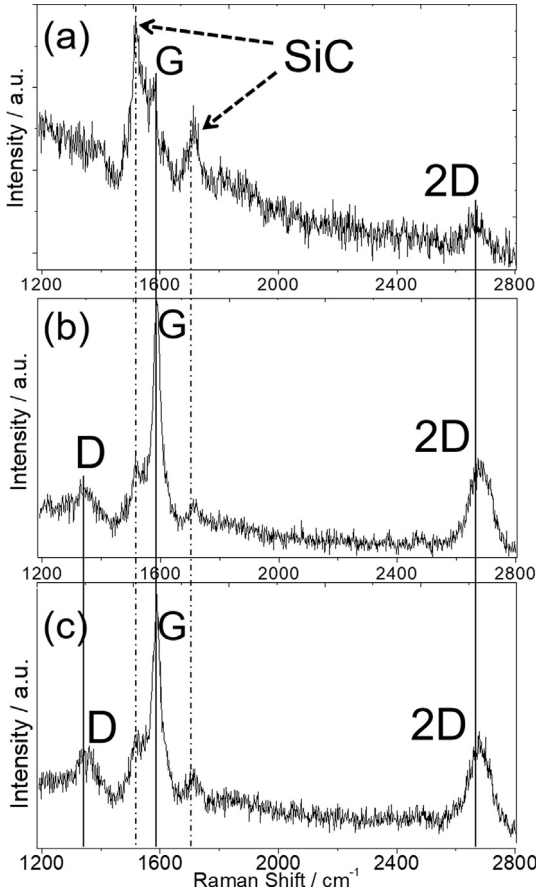

Fig. 2. (a), (b) and (c) Raman spectra measured from the samples shown in Fig. 1(a) and (d) and 1(g), respectively. The D-, G- and 2D-band of graphene and SiC peaks are marked.

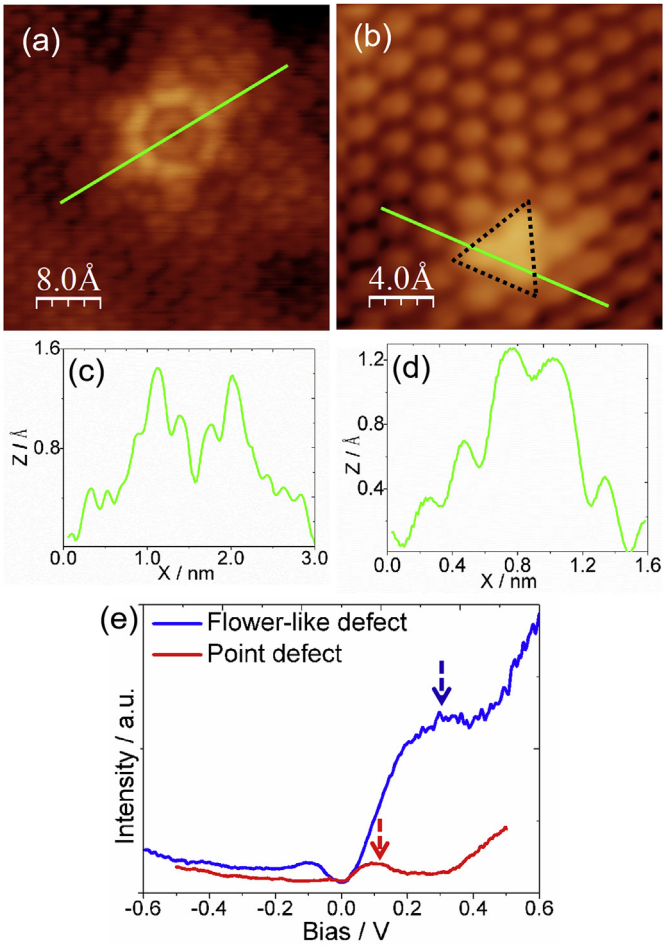

Fig. 3. (a)–(b) Atomic structure of flower-like and point defects on EG. (c) and (d) Height profiles of the two defects acquired from the green lines in (a) and (b), respectively. (e) dI/dV-V curves measured on flower-like (blue) and point defects (red). The scanning conditions for (b) and (c) are I = 100 pA, V = 20 mV. (A colour version of this figure can be viewed online.)

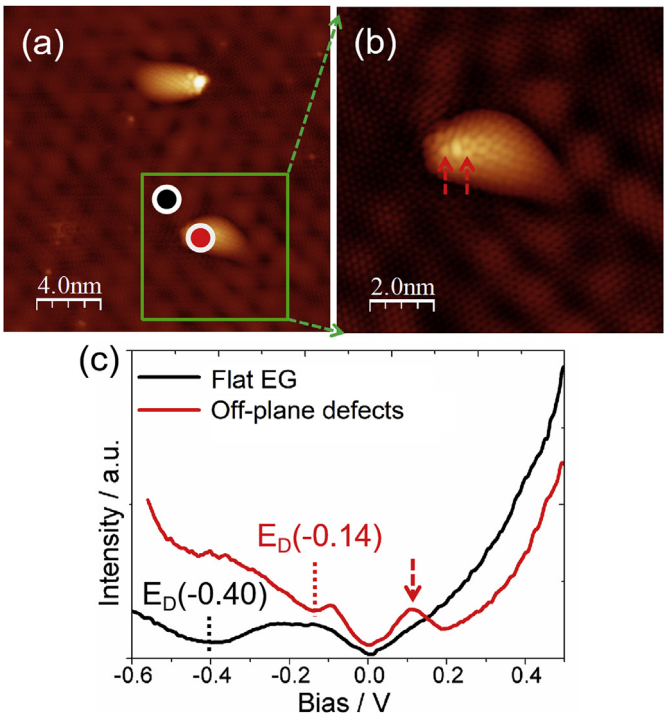

Fig. 4. (a) and (b) Atomically resolved structure of tube-like defects on EG, (b) Zoom-in image from the green square in (a). (c) dI/dV-V curves measured on the flat EG (black dot) and the off-plane defects (red dot). The scanning conditions for (a) and (b) are I = 100 pA, V = 30 mV. (A colour version of this figure can be viewed online.)

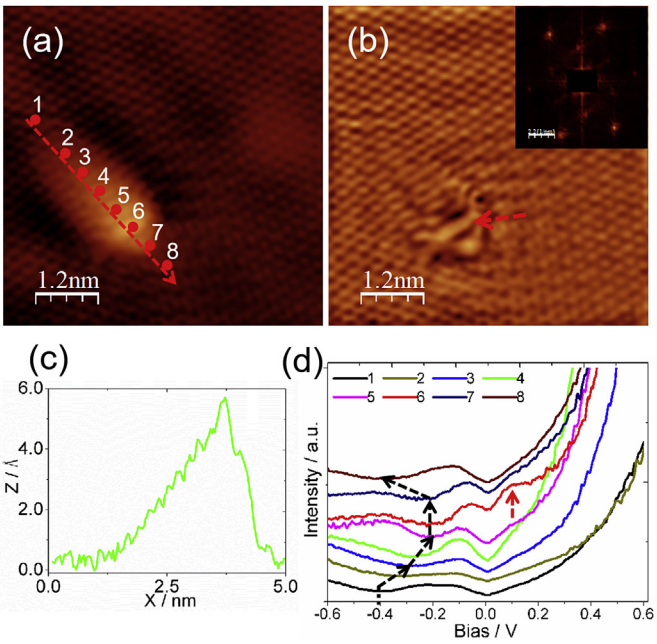

Fig. 5. (a) Atomic structure of tube-like defect on EG. (b) Filtered STM image by the FFT shown in inset. (c) the profile acquired from the red arrow in (a). (d) dI/dV-V curves measured on the eight points along the red arrow in (a), the shift of Dirac point is marked by the black arrows. The scanning conditions for (a) are I = 100 pA, V = 30 mV. (A colour version of this figure can be viewed online.)

lattices, $\sqrt{3} \times \sqrt{3}$ patterns are vividly intrigued by strong quantum interference (QI) of electrons [44–46]. It indicates that flower-like defects are rightly on top of the EG layer and have strong influences on the local electronic states. The EG fabricated through thermal decomposition of SiC is not strictly uniform [47,48]. Combined with the atomically resolved STM images [(AB stacking in Fig. 3(b)] and STS spectra, it is speculated that two-layered graphene in average is produced on SiC. The point defective sites can be evidenced by the highlighted pattern and be identified as a triangular shape (black dashed triangle). Fig. 3(c) and (d) show the height profiles along the green lines in Fig. 3(a) and (b), exhibiting symmetric shapes of the defects. Fig. 3(e) depicts the STS spectra on top of the center of the defects. A broad peak appears in the range of 0 V–0.2 V, corresponding to the defective states above Fermi level (unoccupied states) [43].

Fig. 4(a) displays the ridged morphology of two tube-like defects on EG, and Fig. 4(b) displays the atomically resolved structure of highlighted nano-tube. Due to the ridged structure, no QI-induced $\sqrt{3} \times \sqrt{3}$ patterns is formed around the off-plane defective sites [49]. So the defective graphene lattices as highlighted by the red arrows are atomically resolved, which are similar to the S-W defects on graphene [50]. Because of the missing carbon atoms, graphene lattices are not closed in one flat plane. Thus, ridged structures are easily induced by dislocations and exhibit as off-plane defects on EG Ref. [27]. Fig. 4(c) displays the STS obtained on the regions marked by black and red dots in Fig. 4(a), respectively. Although both of them exhibit the typical local electronic states of EG, there is some difference caused by the tube-like defect. For the flat EG (black curve), the Dirac point (black dashed line) is located at −0.40 V, however, for the defective sites on the nano-tube (red curve), the Dirac point (red dashed line) is located at −0.14 V. The shift of Dirac point toward Fermi level is due to the decoupling of EG layer from SiC and thus lowered n-doping caused by the ridged structure [51]. Similar to the STS spectra measured on the flower-like and point defects in Fig. 3(e), there is also a broad peak in the range of 0 V–0.2 V as indicated by the red arrow, indicating the defective states above Fermi level.

Local electronic structures, near the defective sites on nano-tube, are sensitively changed, dependent on the STS measurement positions. Fig. 5(a) shows the atomically resolved structure of one tube-like defect. Fig. 5(b) reveals further detailed configuration of the defective sites on the nano-tube filtered through the fast Fourier transform (FFT). As designated by the red arrow, the defective sites are located at the top site of the nano-tube. The profile of Fig. 5(c) acquired along the red arrow marked in Fig. 5(a) depicts the gradually increasing sub-nanometer height of the nano-tube. Fig. 5(d) shows the local electronic states measured on the eight points along the nano-tube, and the dI/dV-V curves on points 1 and 8 exhibit the typical features of flat EG Ref. [52], on which the Dirac points are located at -0.40 V. From positions 2 to 7, the Dirac point is gradually shifted from -0.32 V to -0.19 V, suggesting the decoupling of EG layer from SiC substrate owing to the ridged structure. This is consistent with the gradually increased height of nano-tube. As indicated by the red arrow, the defective states are measured only on the top site (position 6) of the nano-tube, which is consistent with the STM image and the height profile. Fig. 6 displays the structure and electronic states of the elongated tube-like defects, and similar features to those of the tube-like ones are identified. Fig. 6(a) displays the detailed structure of nano-tubes on EG. Correspondingly, the defective sites on the nano-tubes always exhibit as bright spots, and the height of the nano-tube is also in sub-nanometer as depicted by the profiles shown in Fig. 6(b). Fig. 6(c) shows the STS spectra at the positions marked on the elongated defects. The Dirac point is located at -0.15 V, that is, it is shifted towards the lower value, indicating the decoupling feature of EG layer from SiC. The red dI/dV-V curve is measured on nano-tubes indicated by the red arrows in Fig. 6(a). The defective states appear in the range of 0 V to 0.2 V [marked by red arrows in

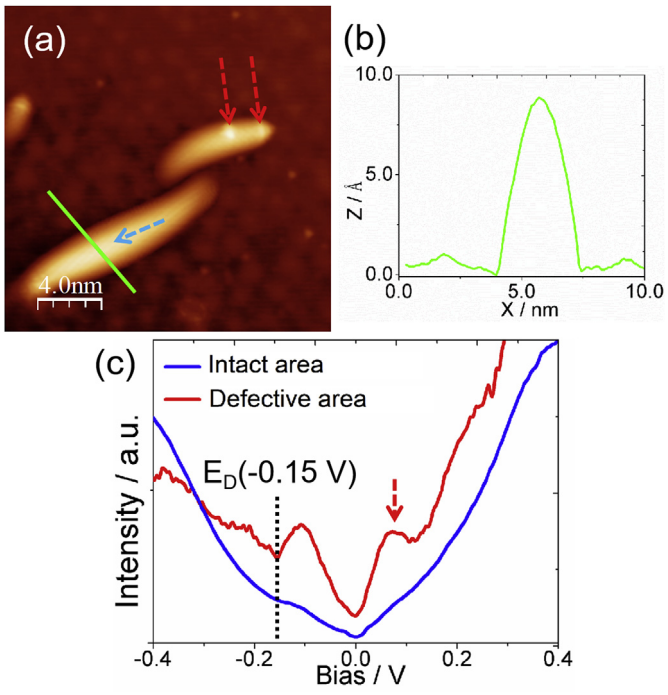

Fig. 6. (a) and (b) Atomic structure of tube-like defects and the profile. (c) dI/dV-V curves show the local electronic states of intact nano-tube (blue) and defective site on nano-tube (red). The scanning conditions for (a) are I = 100 pA, V = 50 mV. (A colour version of this figure can be viewed online.)

Fig. 6(c)], which are similar to those on the red curves in Figs. 4(c) and 5(d). The blue dI/dV-V curve is measured on the intact nano-tube indicated by the blue arrow in Fig. 6(a), a nearly free standing feature is exhibited. There is no defective sites around the intact ridged structure, so the localized defective states did not appear.

Essentially, the shift of Dirac point of the EG on SiC is mainly due to the intrinsic charge transfer from the substrate to EG as well as electronic doping in EG Ref. [53]. The doping level is closely related to the distance between EG and SiC, e.g., the doping effect will be weakened owing to decoupling effect if the EG is far away from the SiC substrate [54]. Local deformation and lattice strain might modulate the electronic states of EG as well [55], however, it is much weaker than the charge transfer doping effect on the shift of Dirac point. Specifically, the unoccupied states in the STS [Figs. 4(c) and Fig. 5(d)] are most likely from the dangling bonds of carbon atoms [56]. As displayed by the high-resolution STM images, tube-like off-plane defects are caused by dislocations in the lattice, and thus the carbon atoms with dangling bonds always appear at the higher end of tube-like defect [Figs. 5(b) and 4(b)]. The peak of the unoccupied state in STS becomes weaker and weaker when the tip is moved away from the high end of the tube-like defect. The peak shape is similar to but indeed not the Van Hove singularity of twisted bilayer graphene, since the energy resolution of the system at 77 K is not high enough to observe the Van Hove singularity. It is also not likely due to the Kondo effect because no magnetic impurities are involved, and the measurement is done at higher temperature.

Fig. 7 schematically displays the process of Bi-induced defects in the EG. Fig. 7(a) shows the model of SiC substrate covered with Bi. Most of Bi atoms are sublimated during thermal annealing, but a few Bi atoms left on the surface will participate in the formation of the EG layer [Fig. 7(b)]. However, the residual Bi atoms will also be sublimated after post-annealing at high temperature, resulting in defects in the EG lattice. Fig. 7(c) and (d) show the models of in-plane and off-plane defects in EG layer, respectively. It is deduced that the pre-covered Bi atoms on SiC could facilitate the defect formation of graphene since they participate in the growth of graphene during annealing. It was demonstrated that the Bi atoms on SiC could merge into the graphene lattice as interstitial dopants during annealing at moderate temperatures [35]. Since the ion radius of Bi is larger than C, the dislocations and other non-6-member-rings might be induced in the lattice, and Bi dopants will be sublimated during post annealing at elevated temperature, resulting in vacancies and dislocations. If the post annealing at higher temperature is prolonged, the carbon dangling bonds at the in-plane defects will be eliminated, thus lower the concentration of in-plane defects. The irreparable in-plane defect complexes will lead to local bumps and off-plane defects. In brief, Bi covered on SiC can induce the formation of defects in EG layer, and the defect types can be controllably tuned by changing the post annealing parameters. Accordingly, the physical properties of graphene could be tune by defect engineering.

4. Conclusions

Both in-plane and off-plane defects in epitaxial graphene on SiC are produced by introducing Bi in the graphene growth process and tuned by controlling the post-annealing parameters. The atomically resolved structures and electronic states of Bi-induced defects on EG are studied. The in-plane depressions under large bias are caused by the grain boundary loops and defects, of which the flower-like and triangle patterns are evidenced under small bias.

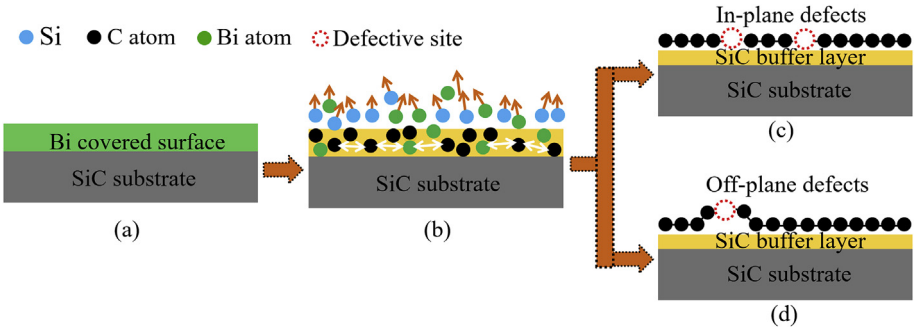

Fig. 7. (a) The model of SiC substrate covered with Bi. (b) the possible reactions between Bi and C atoms during the decomposition of SiC. (c) and (d) the models of in-plane and off-plane defects in EG layer. (A colour version of this figure can be viewed online.)

Tube-like defects are always evidenced on EG, regardless of the bias voltage. Defective states around Fermi level (0–0.2 V) are identified by STS. The Dirac point shifts along the off-plane defects due to the gradually increasing height of the ridged structure and thus the decoupling of EG layer from the substrate to some degree. The results shine light on the defect engineering of high quality epitaxial graphene on SiC substrate as well as on the potential applications in electronics.

Acknowledgements

This work was jointly supported by National Natural Science Foundation of China (Grant Nos. 51601142, 51771144, 51471130), China Postdoctoral Science Foundation (2016M592785), National Key R&D Program of China (2017YFA0206202), Natural Science Foundation of Shaanxi Province (No. 2017JZ015), Fundamental Research Funds for the Central Universities and Collaborative Innovation Center of Suzhou Nano Science and Technology.

Appendix A. Supplementary data

Supplementary data to this article can be found online at https://doi.org/10.1016/j.carbon.2019.02.014.

References

[1] G.M. Rutter, J.N. Crain, N.P. Guisinger, T. Li, P.N. First, J.A. Stroscio, Scattering and interference in epitaxial graphene, Science 317 (2007) 219–222.
[2] L. Simon, C. Bena, F. Vonau, D. Aubel, H. Nasrallah, M. Habar, et al., Symmetry of standing waves generated by a point defect in epitaxial graphene, Eur. Phys. J. B 69 (2009) 351–355.
[3] T.V. Alencar, M.G. Silva, L.M. Malard, A.M. de Paula, Defect-induced supercollision cooling of photoexcited carriers in graphene, Nano Lett. 14 (2014) 5621–5624.
[4] J. Ekspong, N. Boulanger, E. Gracia-Espino, Surface activation of graphene nanoribbons for oxygen reduction reaction by nitrogen doping and defect engineering: an ab initio study, Carbon 137 (2018) 349–357.
[5] H.C. Lee, H. Bong, M.S. Yoo, M. Jo, K. Cho, Copper-vapor-assisted growth and defect-healing of graphene on copper surfaces, Small 14 (2018) 1801181.
[6] L. Jaber-Ansari, K.P. Puntambekar, H. Tavassol, H. Yildirim, A. Kinaci, R. Kumar, et al., Defect evolution in graphene upon electrochemical lithiation, ACS Appl. Mater. Interfaces 6 (2014) 17626–17636.
[7] A. Zandiatashbar, G.H. Lee, S.J. An, S. Lee, N. Mathew, M. Terrones, et al., Effect of defects on the intrinsic strength and stiffness of graphene, Nat. Commun. 5 (2014) 3186.
[8] C.G. Wang, L. Lan, Y.P. Liu, H.F. Tan, Defect-guided wrinkling in graphene, Comput. Mater. Sci. 77 (2013) 250–253.
[9] A.W. Robertson, K. He, A.I. Kirkland, J.H. Warner, Inflating graphene with atomic scale blisters, Nano Lett. 14 (2014) 908–914.
[10] J. Lei, Y. Hu, Z. Liu, G.J. Cheng, K. Zhao, Defects mediated corrosion in graphene coating layer, ACS Appl. Mater. Interfaces 9 (2017) 11902–11908.
[11] A. Hashimoto, K. Suenaga, A. Gloter, K. Urita, S. Iijima, Direct evidence for atomic defects in graphene layers, Nature 430 (2004) 870–873.
[12] G. Xie, R. Yang, P. Chen, J. Zhang, X. Tian, S. Wu, et al., A general route towards defect and pore engineering in graphene, Small 10 (2014) 2280–2284.
[13] C.A. Polanco, L. Lindsay, Ab initio phonon point defect scattering and thermal transport in graphene, Phys. Rev. B 97 (2018), 014303.
[14] G. Nanda, S. Goswami, K. Watanabe, T. Taniguchi, P.F. Alkemade, Defect control and n-doping of encapsulated graphene by helium-ion-beam irradiation, Nano Lett. 15 (2015) 4006–4012.
[15] Z. Yang, S. Bhowmick, F.G. Sen, A. Banerji, A.T. Alpas, Roles of sliding-induced defects and dissociated water molecules on low friction of graphene, Sci. Rep. 8 (2018) 121.
[16] V.S. Anithaa, R. Shankar, S. Vijayakumar, Adsorption of Mn atom on pristine and defected graphene: a density functional theory study, J. Mol. Model. 23 (2017) 132.
[17] D.E. García-Rodríguez, L.H. Mendoza-Huizar, C. Díaz, A DFT study of Cu nanoparticles adsorbed on defective graphene, Appl. Surf. Sci. 412 (2017) 146–151.
[18] X.-L. Ye, J. Cai, X.-D. Yang, X.-Y. Tang, Z.-Y. Zhou, Y.-Z. Tan, et al., Quantifying defect-enhanced chemical functionalization of single-layer graphene and its application in supramolecular assembly, J. Mater. Chem. 5 (2017) 24257.
[19] Y. Zhou, A. Lii-Rosales, M. Kim, M. Wallingford, D. Jing, M.C. Tringides, et al., Defect-mediated, thermally-activated encapsulation of metals at the surface of graphite, Carbon 127 (2018) 305–311.
[20] M. Büttner, P. Choudhury, J. Karl Johnson, J.T. Yates, Vacancy clusters as entry ports for cesium intercalation in graphite, Carbon 49 (2011) 3937–3952.
[21] Q. Chu, L. Li, C. Zhu, Y. Zang, S. Lin, Y. Han, Preparation of SiC/Ge/graphene heterostructure on 4H-SiC(0001), Mater. Lett. 211 (2018) 133–137.
[22] G. Zamborlini, M. Imam, L.L. Patera, T.O. Mentes, N. Stojic, C. Africh, et al., Nanobubbles at GPa pressure under graphene, Nano Lett. 15 (2015) 6162–6169.
[23] K. Ienaga, T. Iimori, K. Yaji, T. Miyamachi, S. Nakashima, Y. Takahashi, et al., Modulation of electron-phonon coupling in one-dimensionally nanorippled graphene on a macrofacet of 6H-SiC, Nano Lett. 17 (2017) 3527–3532.
[24] N. Levy, S.A. Burke, K.L. Meaker, M. Panlasigui, A. Zettl, F. Guinea, et al., Strain-induced pseudo-magnetic fields greater than 300 tesla in graphene nanobubbles, Science 329 (2010) 544–547.
[25] M. Lusk, L. Carr, Nanoengineering defect structures on graphene, Phys. Rev. Lett. 100 (2008) 175503.
[26] S. Kumar, A. Kumar, A. Tripathi, C. Tyagi, D.K. Avasthi, Engineering of electronic properties of single layer graphene by swift heavy ion irradiation, J. Appl. Phys. 123 (2018) 161533.
[27] F. Banhart, J. Kotakoski, A.V. Krasheninnikov, Structural defects in graphene, ACS Nano 5 (2010) 26–41.
[28] X. Wang, Y. Chen, G. Wu, J. Wang, B. Tian, S. Sun, et al., Graphene Dirac point tuned by ferroelectric polarization field, Nanotechnology 29 (2018) 134002.
[29] C. Strasser, B.M. Ludbrook, G. Levy, A.J. Macdonald, S.A. Burke, T.O. Wehling, et al., Long-versus short-range scattering in doped epitaxial graphene, Nano Lett. 15 (2015) 2825–2829.
[30] X. Liu, C.-Z. Wang, H.-Q. Lin, M. Hupalo, P.A. Thiel, K.-M. Ho, et al., Structures and magnetic properties of Fe clusters on graphene, Phys. Rev. B 90 (2014) 155444.
[31] Z. Bai, L. Zhang, L. Liu, Improving low-energy boron/nitrogen ion implantation in graphene by ion bombardment at oblique angles, Nanoscale 8 (2016) 8761–8772.
[32] S. Standop, O. Lehtinen, C. Herbig, G. Lewes-Malandrakis, F. Craes, J. Kotakoski, et al., Ion impacts on graphene/Ir(111): interface channeling, vacancy funnels, and a nanomesh, Nano Lett. 13 (2013) 1948–1955.
[33] Z. Auzar, Z. Johari, S.H. Sakina, N.E. Alias, Adsorption site of gas molecules on defective armchair graphene nanoribbon formed through ion bombardment, J. Electron. Mater. 47 (2017) 1208–1217.
[34] X. Liu, T. Hu, Y. Miao, D. Ma, Z. Yang, F. Ma, et al., Substitutional doping of Ag into epitaxial graphene on 6H-SiC substrates during thermal decomposition, Carbon 104 (2016) 233–240.
[35] T. Hu, Q. Fang, X. Zhang, X. Liu, D. Ma, R. Wei, et al., Enhanced n-doping of epitaxial graphene on SiC by bismuth, Appl. Phys. Lett. 113 (2018), 011602.
[36] B. Sharma, T. Schumann, M.H. de Oliveira, J.M.J. Lopes, Controlled synthesis and characterization of multilayer graphene films on the C-face of silicon carbide, Phys. Status Solidi A-Appl. Mat. 214 (2017) 1600721.
[37] K.V. Emtsev, A. Bostwick, K. Horn, J. Jobst, G.L. Kellogg, L. Ley, et al., Towards wafer-size graphene layers by atmospheric pressure graphitization of silicon carbide, Nat. Mater. 8 (2009) 203–207.
[38] M. Kruskopf, D.M. Pakdehi, K. Pierz, S. Wundrack, R. Stosch, T. Dziomba, et al., Comeback of epitaxial graphene for electronics: large-area growth of bilayer-free graphene on SiC, 2D Mater. 3 (2016), 041002.
[39] Y. Yang, L.I. Huang, Y. Fukuyama, F.H. Liu, M.A. Real, P. Barbara, et al., Low carrier density epitaxial graphene devices on SiC, Small 11 (2015) 90–95.
[40] W. Tian, W. Li, W. Yu, X. Liu, A review on lattice defects in graphene: types, generation, effects and regulation, Micromachines 8 (2017) 163.
[41] T.W. Hu, F. Ma, D.Y. Ma, D. Yang, X.T. Liu, K.W. Xu, et al., Evidence of atomically resolved 6×6 buffer layer with long-range order and short-range disorder during formation of graphene on 6H-SiC by thermal decomposition, Appl. Phys. Lett. 102 (2013) 171910.
[42] I. Horcas, R. Fernandez, J.M. Gomez-Rodriguez, J. Colchero, J. Gomez-Herrero, A.M. Baro, WSXM: a software for scanning probe microscopy and a tool for nanotechnology, Rev. Sci. Instrum. 78 (2007), 013705.
[43] E. Cockayne, G. Rutter, N. Guisinger, J. Crain, P. First, J. Stroscio, Grain boundary loops in graphene, Phys. Rev. B 83 (2011) 195425.
[44] L. Daukiya, C. Mattioli, D. Aubel, S. Hajjar-Garreau, F. Vonau, E. Denys, et al., Covalent functionalization by cycloaddition reactions of pristine defect-free graphene, ACS Nano 11 (2017) 627–634.
[45] C. Park, H. Yang, A.J. Mayne, G. Dujardin, S. Seo, Y. Kuk, et al., Formation of unconventional standing waves at graphene edges by valley mixing and pseudospin rotation, Proc. Natl. Acad. Sci. U. S. A 108 (2011) 18622–18625.
[46] L. Chen, P. Cheng, K. Wu, Quasiparticle interference in unconventional 2D systems, J. Phys.-Condes. Matter 29 (2017) 103001.
[47] S.W. Poon, W. Chen, A.T. Wee, E.S. Tok, Growth dynamics and kinetics of monolayer and multilayer graphene on a 6H-SiC(0001) substrate, Phys. Chem. Chem. Phys. 12 (2010) 13522–13533.
[48] W.A. de Heer, C. Berger, M. Ruan, M. Sprinkle, X. Li, Y. Hu, et al., Large area and structured epitaxial graphene produced by confinement controlled sublimation of silicon carbide, Proc. Natl. Acad. Sci. U. S. A 108 (2011) 16900–16905.
[49] T. Hu, D. Ma, F. Ma, K. Xu, P.K. Chu, Direct and diffuse reflection of electron waves at armchair edges of epitaxial graphene, RSC Adv. 3 (2013) 25735.
[50] Y. Ren, G. Cao, Effect of geometrical defects on the tensile properties of graphene, Carbon 103 (2016) 125–133.
[51] T. Hu, H. Bao, S. Liu, X. Liu, D. Ma, F. Ma, et al., Near-free-standing epitaxial graphene on rough SiC substrate by flash annealing at high temperature, Carbon 120 (2017) 219–225.
[52] W.-J. Zuo, J.-B. Qiao, D.-L. Ma, L.-J. Yin, G. Sun, J.-Y. Zhang, et al., Scanning tunneling microscopy and spectroscopy of twisted trilayer graphene, Phys.

Rev. B 97 (2018), 035440.
[53] J. Ristein, S. Mammadov, T. Seyller, Origin of doping in quasi-free-standing graphene on silicon carbide, Phys. Rev. Lett. 108 (2012) 246104.
[54] S. Mammadov, J. Ristein, J. Krone, C. Raidel, M. Wanke, V. Wiesmann, et al., Work function of graphene multilayers on SiC(0001), 2D Mater. 4 (2017), 015043.
[55] C. Si, Z. Sun, F. Liu, Strain engineering of graphene: a review, Nanoscale 8 (2016) 3207–3217.
[56] T. Kondo, Y. Honma, J. Oh, T. Machida, J. Nakamura, Edge states propagating from a defect of graphite: scanning tunneling spectroscopy measurements, Phys. Rev. B 82 (2010) 153414.